Pergamon

Int. J. Heat Mass Transfer. Vol. 37, No. 3, pp. 499–509, 1994

0017-9310/94 $6.00+0.00

Enhancement of heat transfer for a tube with an inner tube insertion

WU-SHUNG FU and CHING-CHI TSENG
Department of Mechanical Engineering, National Chiao Tung University, Hsinchu 30050, Taiwan, R.O.C.

(*Received* 4 *August* 1992 *and in final form* 22 *March* 1993)

Abstract—A numerical study of flow field and heat transfer in a heated circular tube with an inner tube inserted has been investigated. Due to the insertion of the inner tube, part of the fluid is deviated from the original path to the heated tube which results in the increase of heat transfer rate from the heated wall. The Projection method is adopted to predict the flow field and three different types of inner tube, (1) straight tube, (2) contraction–enlargement tube and (3) enlargement–contraction tube, are considered. The calculations are performed for Reynolds numbers of 100, 500, 1000, and Prandtl numbers of 0.1, 0.7, 7 and 10. The results show that, except at very low Peclet number, the heat transfer rate of the heated tube increases when an inner tube is inserted. About 50% increase in heat transfer rate can be achieved under the condition of constant pumping power evaluation and twice the heat transfer rate than for the empty tube can be achieved under the condition of constant flow rate evaluation.

INTRODUCTION

SMOOTH pipes are quite often employed in industrial applications, especially in heat-exchange equipment. However, due to the formation of a boundary layer near the pipe wall, which reduces the heat transfer coefficient, many different methods are developed to augment the heat transfer of the smooth pipe without severe pressure drop. These methods summarized by Bergles [1, 2] include passive methods, which require no external power such as treated surfaces, extended surfaces, swirl flow devices, and active schemes, which require external power such as surface vibration, fluid vibration, injection and suction. Extended surfaces are often used and many investigations have been presented in the open literature. For example, Nguyen *et al.* [3] studied the flow field and conjugate heat transfer in rib-roughened tubes numerically and found that the size of recirculation zone and pressure drop both increase with increasing Reynolds number and rib height. The heat transfer intensifies only at high Prandtl number owing to the influence of downstream recirculation. Gee and Webb [4] performed an experiment to depict the phenomena of a helically rib-roughened tube and tried to find the optimal helix angle. Their results showed that the heat transfer performance for a tube with helical rib is better than the tube with transverse-rib. Patankar *et al.* [5] analyzed the heat transfer of a finned tube in turbulent flow and found that turbulence intensifies heat transfer significantly. Rowly and Patankar [6] investigated the heat transfer of tubes in laminar flow with internal circumferential fins by numerical methods and found that the recirculation behind the fin leads to a severe pressure drop. The fin deviates the fluids away from the hot surface which makes the heat-transfer augmentation occur at high Prandtl number only.

Other studies using varying cross-section to enhance the heat transfer rate of tubes were also undertaken. Sparrow and Prata [7] investigated the phenomena of a converging–diverging tube by experimental and numerical methods. The enhancement of heat transfer occurs at high Prandtl number, but the accompanied pressure drop is even higher. The study of an annulus of periodically varying cross-section was analyzed by Prata and Sparrow [8]. The results, which compared with the uniform cross-section annulus, revealed that the annulus with an undulated cross-section is a better shape for heat transfer because the increase of heat transfer is higher than the increase of pressure drop at high Prandtl number, but for low Prandtl number the performance depends on Reynolds number and geometrical parameters. Agrawal and Sengupta [9] employed the vorticity–stream function to analyze the phenomena of a blocked annulus. They showed that although the blockage can raise the average Nusselt number, the increase of pressure drop is about an order of magnitude higher than the increase of Nusselt number.

From the literature above, the optimal device is expected to lead more working fluid passing through the heated surface to increase heat transfer, and its geometry to be as simple as possible in order to decrease the accompanied increase of pressure drop and production cost. Based upon this belief, the present work employed the numerical projection method to investigate the heat-transfer enhancement by inserting an inner-tube into a straight tube. The inner tube deflects the fluid to the hot wall to elevate the heat transfer coefficient but does not increase the pressure drop seriously because of the simple configuration of the inner tube. There were five different types of inner tube employed in this study: Type I—small tube, Type II—medium size tube, Type III—large tube (these

NOMENCLATURE

c	specific heat [J kg^{-1} K^{-1}]
d	diameter of outer tube [m]
l	total tube length [m]
f	pressure drop coefficient
k	thermal conductivity [W m^{-1} K^{-1}]
$\dot{m}$	mass flow rate [kg s^{-1}]
Nu	Nusselt number
P	dimensionless pressure ($p/\rho u_m^2$)
Pe	Peclet number, $Re \cdot Pr$
PP	pumping power (equation (17))
Pr	Prandtl number, ν/α
Q_{in}	heat transfer into the flow from the hot wall [W]
Q_{out}	energy at the tube outlet [W]
Re	Reynolds number, $u \cdot d/\nu$
r, x	radial and axial coordinates
R, X	dimensionless radial and axial coordinates
Rm	ratio of deviation (%)
r_0	radius of outer tube [m]
r_1, r_2	radii of front and rear inner tube [m]
u, v	axial and radial velocities [m s^{-1}]
u_m	mean axial velocity [m s^{-1}]
U, V	dimensionless axial and radial velocities
T	temperature [K]
T_b	bulk temperature, $(1/\dot{m}_t)\int_0^{r_0} \rho \cdot u(r) Tr\, dr$ [K].

Greek symbols

α	thermal diffusivity [m^2 s^{-1}]
θ	dimensionless temperature, $(T-T_C)/(T_H-T_C)$
ν	kinematic viscosity [m^2 s^{-1}]
ρ	density [kg m^{-3}]
$\vec{\phi}$	velocity vector.

Subscripts

C	low temperature
H	high temperature
o	empty tube
s	constant pumping power condition
x	local value.

Superscript

$\bar{}$	average value.

three are in the form of straight tubes), Type IV—contraction–enlargement tube and Type V—enlargement–contraction tube. Reynolds numbers of 100, 500, 1000 and Prandtl numbers of 0.1, 0.7, 7, and 10 were considered. It was found that the insertion of the inner tube is of little help to heat-transfer enhancement at low Peclet number. However, it had an apparent effect at higher Peclet numbers.

The heat-transfer augmentation is inevitably accompanied by increased pressure drop. The former works [3–9] evaluated the heat-transfer performance and pressure drop separately, i.e. based on the constant flow rate condition, which might make the performance evaluation hard to proceed in a more objective way. For application purposes, the performance evaluation based on the constant pumping power condition is more practical because the combination of pressure drop and heat-transfer coefficient gives a direct description of attainable improvement. Therefore, the heat transfer performances evaluated under the condition of constant pumping power were examined in detail and it was shown that about 50% increase of heat-transfer rate can be achieved when the enlargement–contraction tube was inserted.

PHYSICAL MODEL AND GOVERNING EQUATIONS

Shown in Fig. 1, the physical model includes an outer tube with diameter d, length l and an inner tube. The wall of the outer tube consists of three regions of l_1, l_2 and l_3, where l_1 and l_3 are insulated while l_2 is maintained at a constant high temperature T_H. The inner tube with length l_2 is inserted in the high temperature region, which may deviate the fluid toward the hot wall of the outer tube and augment the heat transfer of the hot wall. The radius of the front-half section of the inner tube is r_1 and the rear-half is r_2. When $r_1 = r_2$, the insertion is a straight tube, $r_1 < r_2$, it is a contraction–enlargement tube and $r_1 > r_2$, an enlargement–contraction tube. At the inlet ($x = 0$), the flow is fully developed and at low temperature

The size of five different types of inner tube

type	r_1	r_2
I	$r_0/3$	$r_0/3$
II	$r_0/2$	$r_0/2$
III	$3r_0/4$	$3r_0/4$
IV	$r_0/3$	$2r_0/3$
V	$2r_0/3$	$r_0/3$

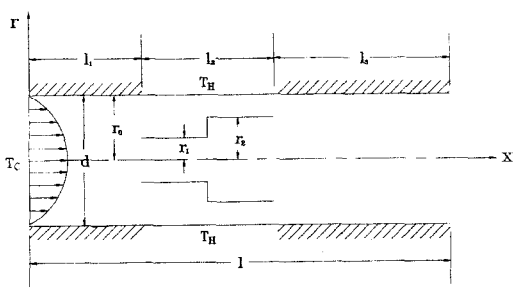

FIG. 1. Physical model.

T_C, while at the exit, there are no further changes of velocity and temperature of fluid. The sizes of five different types of inner tube are shown in Fig. 1. To simplify the analysis, some assumptions are made.

(1) The flow is laminar.
(2) The fluid is Newtonian and incompressible.
(3) The fluid properties are constant.
(4) The wall thickness of the inner tube is infinitely small and the thermal conductivity of the inner tube is much larger than that of the fluid.

With these assumptions, the governing equations in non-dimensional form are written as:

Continuity equation:

$$\frac{\partial(RU)}{\partial X}+\frac{\partial(RV)}{\partial R}=0. \tag{1}$$

X-dir. momentum equation:

$$\frac{1}{R}\left[\frac{\partial}{\partial X}(RU^2)+\frac{\partial}{\partial R}(RUV)\right]=-\frac{\partial P}{\partial X}+\frac{1}{Re\cdot R}\left[\frac{\partial}{\partial X}\left(R\frac{\partial U}{\partial X}\right)+\frac{\partial}{\partial R}\left(R\frac{\partial U}{\partial R}\right)\right]. \tag{2}$$

R-dir. momentum equation:

$$\frac{1}{R}\left[\frac{\partial}{\partial X}(RUV)+\frac{\partial}{\partial R}(RV^2)\right]=-\frac{\partial P}{\partial R}+\frac{1}{Re\cdot R}\left[\frac{\partial}{\partial X}\left(R\frac{\partial V}{\partial X}\right)+\frac{\partial}{\partial R}\left(R\frac{\partial V}{\partial R}\right)\right]-\frac{V}{Re\cdot R^2}. \tag{3}$$

Energy equation:

$$\frac{1}{R}\left[\frac{\partial}{\partial X}(RU\theta)+\frac{\partial}{\partial R}(RV\theta)\right]=\frac{1}{Re\cdot Pr\cdot R}\left[\frac{\partial}{\partial X}\left(R\frac{\partial\theta}{\partial X}\right)+\frac{\partial}{\partial R}\left(R\frac{\partial\theta}{\partial R}\right)\right]. \tag{4}$$

The dimensionless variables are defined as:

$$R=\frac{r}{d},\quad X=\frac{x}{d},\quad L_1=\frac{l_1}{d},\quad L_2=\frac{l_2}{d}$$

$$L_3=\frac{l_3}{d},\quad U=\frac{u}{u_m},\quad V=\frac{v}{u_m},\quad \theta=\frac{T-T_C}{T_H-T_C}$$

$$Re=\frac{u_m\cdot d}{\nu},\quad Pr=\frac{\nu}{\alpha},\quad u_m=\frac{r_0^2}{8\mu}\left(\frac{dp}{dx}\right). \tag{5}$$

Boundary conditions

$$X=0\quad U=2(1-4R^2),\quad V=0,\quad \theta=0 \tag{6a}$$

$$X=1/d\quad \frac{\partial U}{\partial X}=\frac{\partial V}{\partial X}=\frac{\partial\theta}{\partial X}=0 \tag{6b}$$

$$R=0\quad \frac{\partial\theta}{\partial R}=\frac{\partial U}{\partial R}=V=0 \tag{6c}$$

$$L_1<X<L_1+L_2$$

$$R=\frac{r_0}{d}\quad \theta=1, U=V=0 \tag{6d}$$

$$R=\frac{r_1}{d}\quad U=V=0 \tag{6e}$$

$$R=\frac{r_2}{d}\quad U=V=0 \tag{6f}$$

$$0<X<L_1\quad\text{and}\quad L_1+L_2<X<L$$

$$R=\frac{r_0}{d}\quad \frac{\partial\theta}{\partial R}=U=V=0. \tag{6g}$$

NUMERICAL METHOD

The governing equations were solved by a finite-difference procedure. The finite-difference forms were obtained by integrating the equations, coupled with the power law scheme [10], over each control volume. A staggered grid was used for the derivation. The steady-state flow field was predicted by the projection method [11] and the energy equation was solved subsequently. The procedures are described briefly as follows:

(1) Neglect the pressure term in the momentum equation to acquire a velocity $\bar{\phi}^*$:

$$\frac{\bar{\phi}^*-\bar{\phi}^n}{\Delta t}+\bar{A}(\bar{\phi}^n)-\frac{1}{Re}\nabla^2\bar{\phi}^n=0$$

$$\bar{A}(\bar{\phi}^n)=(\bar{\phi}\cdot\nabla)\bar{\phi},\quad(\phi=U,V). \tag{7}$$

(2) Introduce the accurate continuity and momentum equations

$$\nabla\cdot\bar{\phi}^{n+1}=0 \tag{8}$$

$$\frac{\bar{\phi}^{n+1}-\bar{\phi}^n}{\Delta t}+\bar{A}(\bar{\phi}^n)+\bar{\nabla}P^{n+1}-\frac{1}{Re}\nabla^2\bar{\phi}^n=0. \tag{9}$$

Subtract equation (7) from equation (9) to obtain

$$\frac{\bar{\phi}^{n+1}-\bar{\phi}^*}{\Delta t}+\bar{\nabla}P^{n+1}=0. \tag{10}$$

(3) Substitute equation (10) into equation (8) to derive a pressure Poisson equation

$$\nabla^2P^{n+1}=\frac{1}{\Delta t}\nabla\cdot\bar{\phi}^*. \tag{11}$$

(4) Solve equation (11) by SOR method to get pressure and substitute it into equation (10) to obtain the velocity $\bar{\phi}^{n+1}$.
(5) Use $\bar{\phi}^{n+1}$ to solve the energy equation (4).
(6) Repeat (1)–(5) until convergence is achieved.

The convergence criteria were:

Table 1. Comparison of average Nusselt number of type V for $Re = 500$, $Pr = 7$ under different grid system

Grid system X dir. $\times$ R dir.	Average Nusselt number type V
108×72	43.161
108×60	43.433
108×48	43.930
90×72	43.280
90×60	43.550
90×48	44.038
72×72	43.458
72×60	43.725
72×48	44.206

$$\left|\frac{U_{i,j}^n - U_{i,j}^{n-1}}{U_{i,j}^n}\right| < 10^{-5}, \quad \left|\frac{V_{i,j}^n - V_{i,j}^{n-1}}{V_{i,j}^n}\right| < 10^{-5}$$

$$\left|\frac{P_{i,j}^n - P_{i,j}^{n-1}}{P_{i,j}^n}\right| < 10^{-5}, \quad \left|\frac{\theta_{i,j}^n - \theta_{i,j}^{n-1}}{\theta_{i,j}^n}\right| < 10^{-5}$$

$$\left|\frac{Q_{\text{in}}^n - Q_{\text{out}}^n}{Q_{\text{in}}^n}\right| < 10^{-4} \qquad (12)$$

where Q_{in} is the heat transfer into the flow from the hot wall and Q_{out} is the energy at the outlet.

Numerical tests were performed using several grids to calculate the average Nusselt number of type V inner-tube insertion at $Re = 500$ and $Pr = 7$. The results are shown in Table 1 and a grid 90×60 is chosen for all computations. The length of the heating zone (L_2) was 1. In order to exclude the influence of inner tube on the inlet velocity profile and make no further change of velocity at the outlet, $L_1 = 3$ and $L_3 = 5$ were chosen by numerical test. The calculations were performed for Reynolds numbers of 100, 500, 1000, and Prandtl numbers of 0.1, 0.7, 7 and 10.

RESULTS AND DISCUSSION

Figure 2 shows the streamlines for different types of inner tube at $Re = 500$. In Fig. 2(a), the streamlines separate when fluid passes through the inner tube and new boundary layers form on both sides of the inner-tube wall. Since the cross-section area of the inner tube is small, the area occupied by the boundary layer inside the inner tube becomes large which reduces the passage and increases the resistance of flow, respectively. Therefore, more fluid deflects to the outer wall. The increment of the deflection, about 7% more than the empty tube, leads to a greater average velocity between the walls of the inner and outer tubes. The flow pattern in type II is similar to that of type I, while in type III, streamlines still separate when fluid passes through the inner tube. However, the cross-sectional area outside the inner tube decreases contrary to types I and II and deflects more fluid to the inner side of the inner tube.

Figure 2(d) illustrates the streamlines of contraction–enlargement inner tube. Owing to the transverse part of the inner tube, the separation of streamlines at the entrance region of the inner tube are more obvious. In this case, though the front contraction part is placed in the same position as type I, the flow rate deflected to the outer tube does not increase as before. The reason is ascribed to the existence of the transverse part which increases the form drag between the inner and outer walls drastically, and influences the deviation of fluid. In the rear part, because the passage between the walls of inner and outer tubes decreases, the fluid is accelerated and a recirculation zone appears downstream of the transverse part.

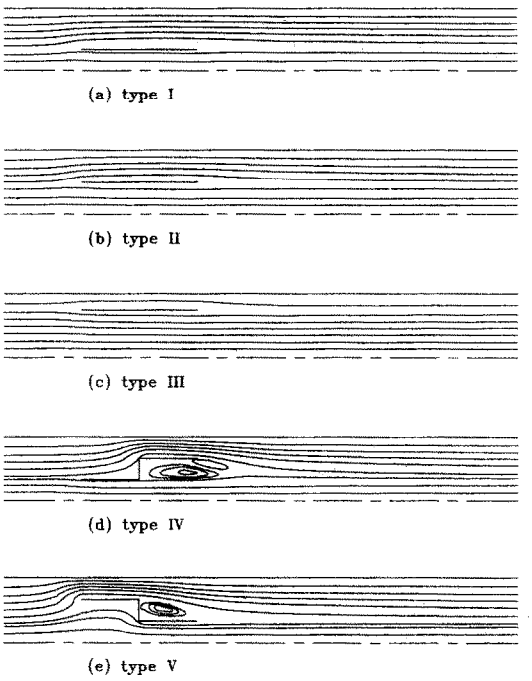

FIG. 2. Streamlines for $Re = 500$ situation.

For the inner tube of type V, the flow pattern variation is more marked than the former ones. Now the enlargement part is placed near the position of type III. Due to the transverse part of the inner tube, the form drag inside the inner tube becomes very large and a large mass of fluid deviates to the outer tube, which results in a greater average velocity between the walls of the inner tube and outer tube, and forms a recirculation zone downstream of the transverse part.

The streamlines for $Re = 1000$ are shown in Fig. 3. Comparing with Fig. 2, the flow fields of types I and II are much alike, since the Reynolds number increases, both the faster fluid velocity and the thinner boundary-layer decrease the deviation of the fluid to the outer tube. For the same reason, the greater inertia and thinner boundary-layer direct a little more fluid relative to the empty tube toward the outer tube in type III. The flow field variations of types IV and V are mainly depicted by the strengthened vortices.

The streamlines for $Re = 100$ are presented in Fig. 4. The smaller Reynolds number thickens the bound-

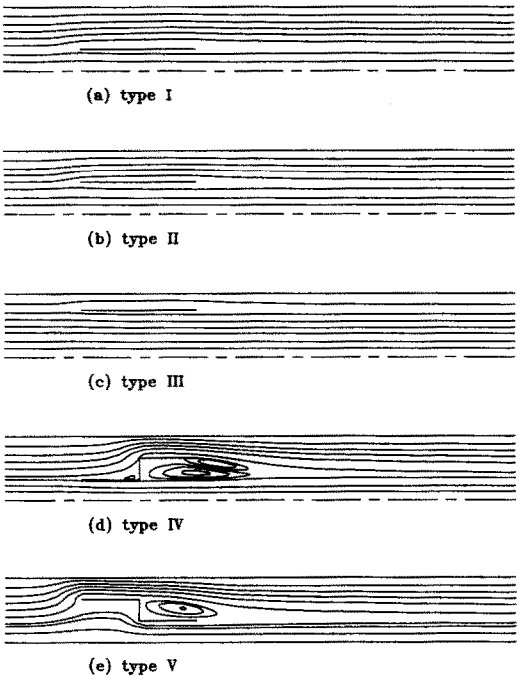

FIG. 3. Streamlines for $Re = 1000$ situation.

ary layer which causes more fluid to deviate to the outer tube for types I and II, but for type III the effect is opposite. The flow fields of types IV and V are similar to those of the former cases, the size of recirculation zone of both types IV and V reduces because of smaller Reynolds number.

The total pressure drop for each case are shown in

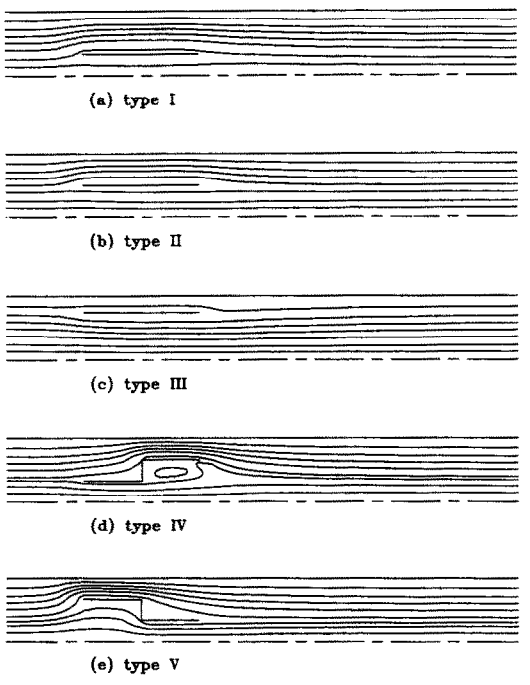

FIG. 4. Streamlines for $Re = 100$ situation.

The coefficients m and n for $f=m(\frac{284.76}{Re})^n$

type	m	n
I	1.44	1
II	1.53	1
III	1.6	0.8
IV	3.5	0.7
V	3.75	0.65

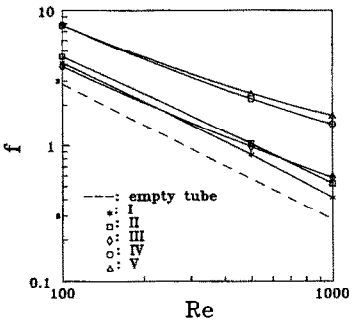

FIG. 5. Pressure drops for different types of inner tube.

Fig. 5. The pressure drop coefficient f is defined as $f = \Delta p/\rho u_m^2$. The coefficient for empty tube is $f = 284.76/Re$, while in the other cases, f can be expressed as $f = m(284.76/Re)^n$, where m, n depend on different cases and are also shown in Fig. 5. The errors for the above formula are within 7%. In types IV and V, the form drag due to the existence of the transverse part of the inner tube increases the pressure drop, so the pressure drops are much higher than for the other types.

Table 2 shows the ratio of mass deviation for different types of inner tube at $Pr = 0.7$. The ratio of deviation Rm is defined as:

$$Rm = \frac{\dot{m}_b - \dot{m}_e}{\dot{m}_t} \times 100\% \tag{13}$$

$\dot{m}_t = \int_0^{r_0} \rho u(r) r \, dr$ total mass flow rate

$\dot{m}_b = \int_{r_1}^{r_0} \rho u(r) r \, dr$ mass flow rate between the inner and outer walls at $x = l_1$

$\dot{m}_e = \int_{r_1}^{r_0} \rho u(r) r \, dr$ mass flow rate between the radii of r_1 and r_0 of the empty tube.

From this Table, relative to the empty tube, the

Table 2. The ratio of deviation R_m

Type	$R_m(Re = 100)$	$R_m(Re = 500)$	$R_m(Re = 1000)$
I	10.804	7.362	5.29
II	9.949	8.242	6.159
III	−7.223	−0.802	1.114
IV	−2.225	−1.2	−1.465
V	47.842	49.509	48.989

flow rate between the inner and outer tubes increases with decreasing Reynolds number for types I and II, and decreases for type III. The flow rate decreases a little for type IV, while increases about 50% for type V. The dependence of flow rate variation on Reynolds number is weak for both types IV and V.

Figure 6 shows the axial velocity profiles at the position of $(1/5)L_2$ downstream from the inner-tube inlet for types I, II and III. At $Re = 100$, the velocity gradient of type III on the hot region of the outer tube is smaller than those of types I and II. Since the insertion position of the inner tube of type II is closer to the outer tube, the gradient is the biggest of these three types. For higher Reynolds number, the velocity gradient of type III increases gradually and becomes the largest among these three types at $Re = 1000$, while that of type I becomes the smallest. These velocities have great influence on heat convection and the smaller the gradient, the less the contribution of convection.

The local Nusselt numbers of different Prandtl numbers for $Re = 100$ are presented in Fig. 7, where the local Nusselt number Nu_x is defined as:

$$Nu_x = \frac{h_x \cdot d}{k}$$

$$h_x = \frac{\dot{q}_x}{(T_H - T_b) \cdot A}, \quad \dot{q}_x = kA \frac{\partial T}{\partial r}\bigg|_{r=r_0}. \tag{14}$$

Shown in Fig. 7(a), except type V, the Nu_x of type II is higher at the beginning of the hot wall of the outer tube but less than that of type I as X increases. The reason is suggested as follows. The fluid is deflected to the outer tube at the inlet of the inner tube for both types I and II, but the inner tube of type II is placed closer to the outer tube and the impingement of the deflected fluid on the outer tube wall is stronger than that of type I, which results in a higher Nu_x. However, because the Peclet number ($Pe = Re \cdot Pr$) is small, the axial heat diffusivity of the fluid cannot be neglected and the heat absorbed by the fluid in the leading edge may be transferred downstream, which retards further heat transfer from the downstream hot wall.

From Table 2, the ratio of deviation of type III is negative and the Peclet number is small which causes the local Nusselt number of type III to be always smaller than that of the empty tube case. As to type IV, in the front contraction part, the ratio of deviation listed in Table 2 is negative so the Nu_x decreases. However, as the fluid enters the enlargement part, the fluids are accelerated and impinge on the hot wall

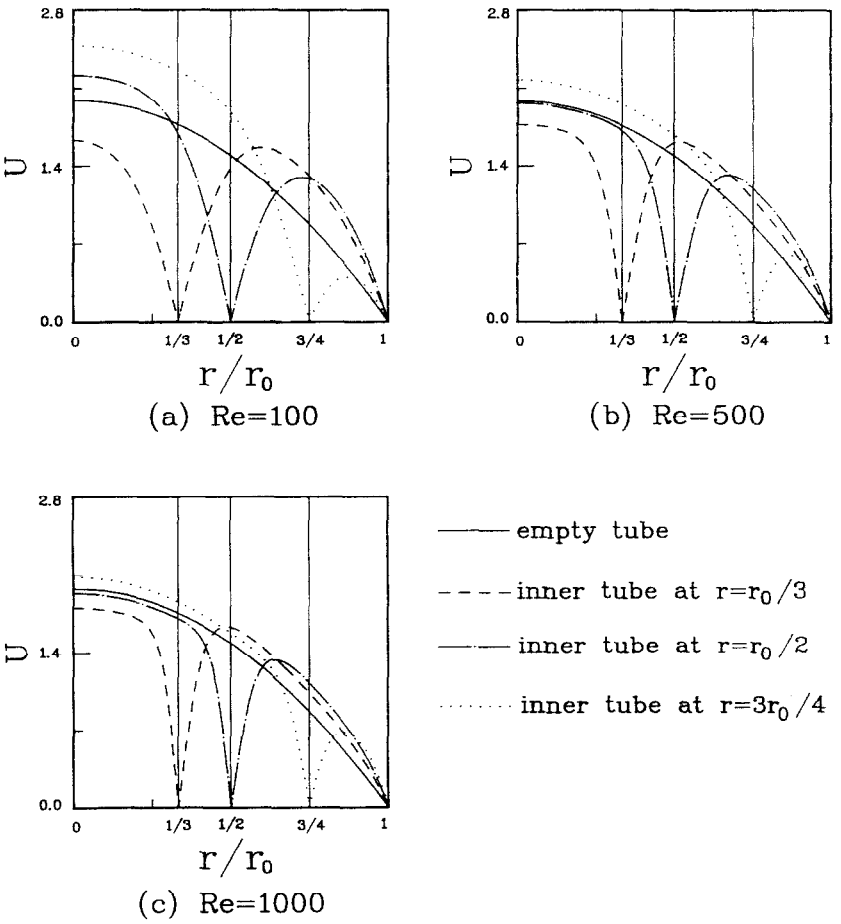

FIG. 6. Axial velocity profiles at $X = L_2/5$ downstream of the inner-tube inlet.

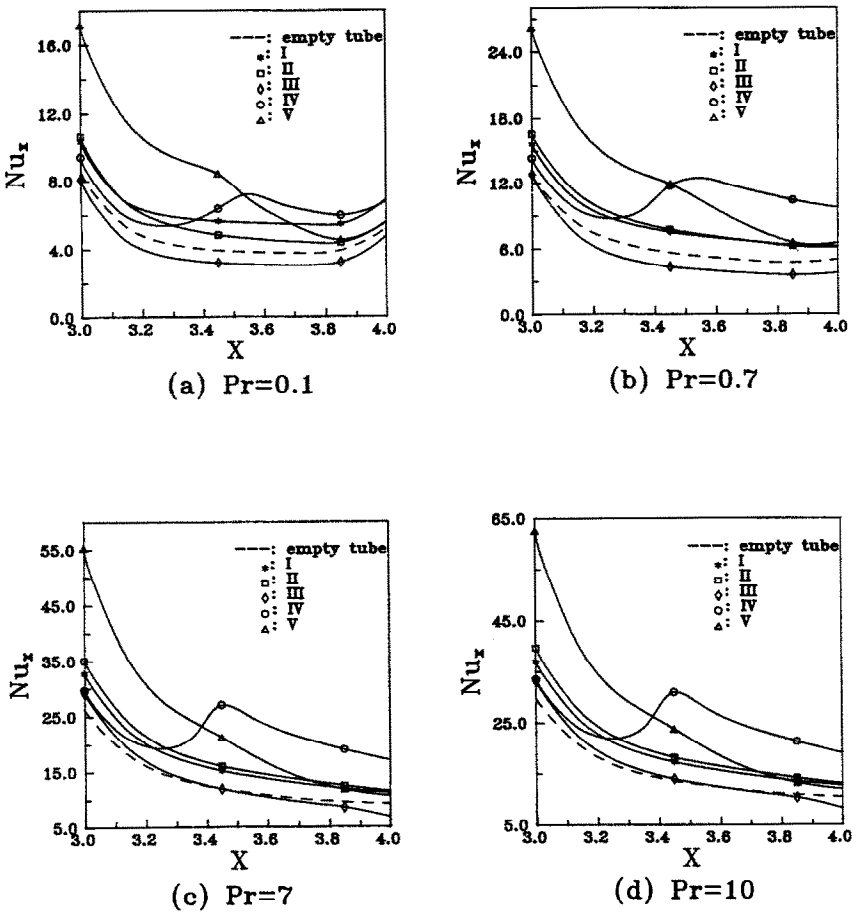

FIG. 7. Local Nusselt number distributions for $Re = 100$ situation.

which leads to a sudden increase of Nu_x and reaches the maximum value. For type V, in the front enlargement region, the fluid is accelerated and impinges on the hot wall which results in a very high Nu_x. When the fluid enters the rear contraction part, the flow velocities reduce causing the decrease of Nu_x. Besides, owing to the very low Peclet number, Nu_x increases in the trailing edge for every case.

Figure 7(b) illustrates the distribution of local Nusselt number for $Pr = 0.7$. Since the Peclet number is higher than for $Pr = 0.1$, the convection effect is intensified and the Nu_x is raised for each case. The trend of the local Nusselt number is similar to Fig. 7(a). The axial heat diffusivity is weakened because of the higher Prandtl number, which leads to the Nu_x of type II to be less than that of type I only in the rear half-part. Also, the increasing of Nu_x at the trailing edge is not significant.

In Fig. 7(c), the Peclet number is much higher. The major heat transfer mechanism changes to convection; axial heat diffusivity is negligible. The phenomena mentioned earlier in Fig. 6 which cause the Nu_x of type II to be larger than that of type I, here for the same reason, cause the Nu_x of type III to be larger than that of the empty tube though the ratio of deviation shown in Table 2 is negative. Figures 7(d) and (c) are much alike.

Figure 8 shows the local Nusselt number distribution for $Re = 500$. The higher Peclet number makes convection stronger and the velocity gradient at the hot wall for type II is steeper than type I, as shown in Fig. 6. It is evident that the Nu_x of type II is always higher than type I. In type III, the flow rate variation is still negative (Table 2), but the velocity gradient on the outer tube shown in Fig. 6 is steeper. Therefore, the stronger convection effects causes the Nu_x in the front region of the hot wall to be higher than that of the empty tube. However, in the rear region of the hot wall, the Nu_x of type III is smaller than that of the empty tube because of the axial heat diffusivity.

In Fig. 8(b), the convection effect is even stronger. Since a greater velocity gradient exists for types II and III than for type I as shown in Fig. 6, the Nu_x of type II is always higher while that of type III is partly higher than that of type I. The local Nusselt number distributions shown in Figs. 8(c) and (d) are much alike as in Fig. 8(b). As described above, high Peclet number makes the Nu_x of type III close to type II.

Figure 9 shows that the high Reynolds number

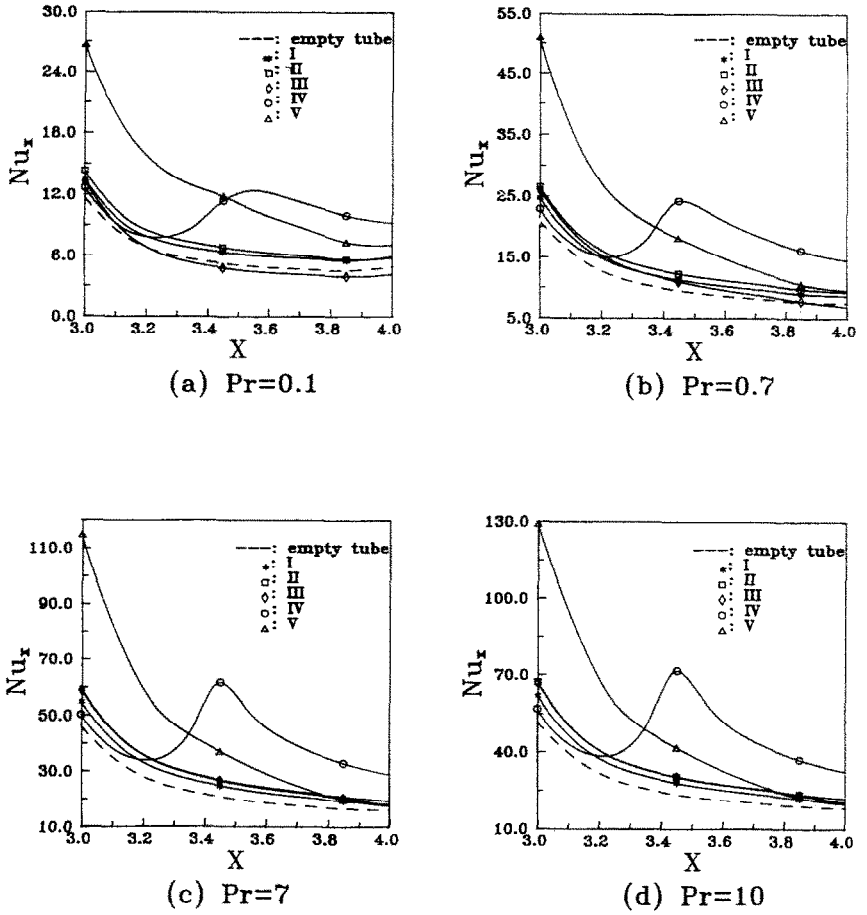

FIG. 8. Local Nusselt number distributions for $Re = 500$ situation.

reduces the ratio of deviation of type II and increases that of type III. The steep velocity gradient of type III shown in Fig. 6 results in a higher Nu_x than those of types I and II. Besides, types IV and V also have much higher Nu_x.

Figure 10 shows the ratio of the average Nusselt numbers $\overline{Nu}$ of the tubes with an inner-tube insertion to the average Nusselt numbers $\overline{Nu}_0$ of the empty tube. $\overline{Nu}$ and $\overline{Nu}_0$ are defined as:

$$\overline{Nu} = \frac{1}{L_2}\int Nu_x \, dX$$

and

$$\overline{Nu}_0 = \frac{1}{L_2}\int Nu_{x0} \, dX. \tag{15}$$

No matter what the Prandtl number is, type V always has the highest ratio, followed by type IV. The ratios for both types IV and V increase with increasing Reynolds number, and the difference between these two types is small for high Prandtl number. The ratios for type II are higher than those of type I except at low Peclet number ($Re = 100$, $Pr = 0.1$), and the ratios for both types reduce as Reynolds number increases. Type III has lower values at low Peclet number and even less than 1 in Figs. 10(a)–(c). As Reynolds and Prandtl number increase, the ratios of type III increase and even surpass types I and II at $Re = 1000$ and Prandtl number greater than 0.1.

From the discussion above, it may be concluded that in order to obtain higher Nusselt numbers, the enlargement–contraction tube may be the better choice, in which the maximum average Nusselt number ratio (about 2.1) can be achieved. The second best is the contraction–enlargement tube. For straight tube insertion, to obtain higher heat transfer rate, the tube should be placed away from the outer wall at low Peclet number ($\simeq 10$), but at high Peclet number, it should be moved toward the outer wall.

The heat transfer performance evaluated by $\overline{Nu}/\overline{Nu}_0$ is made under the condition of constant Reynolds number, i.e. under the condition of constant mass flow rate. However, in view of industry applications, it is more reasonable to evaluate the performance under the condition of constant pumping power. Therefore, the constant pumping power method employed in refs. [12, 13] is also adopted here to assess the degree of improvement of heat transfer performance for different types of inner tube.

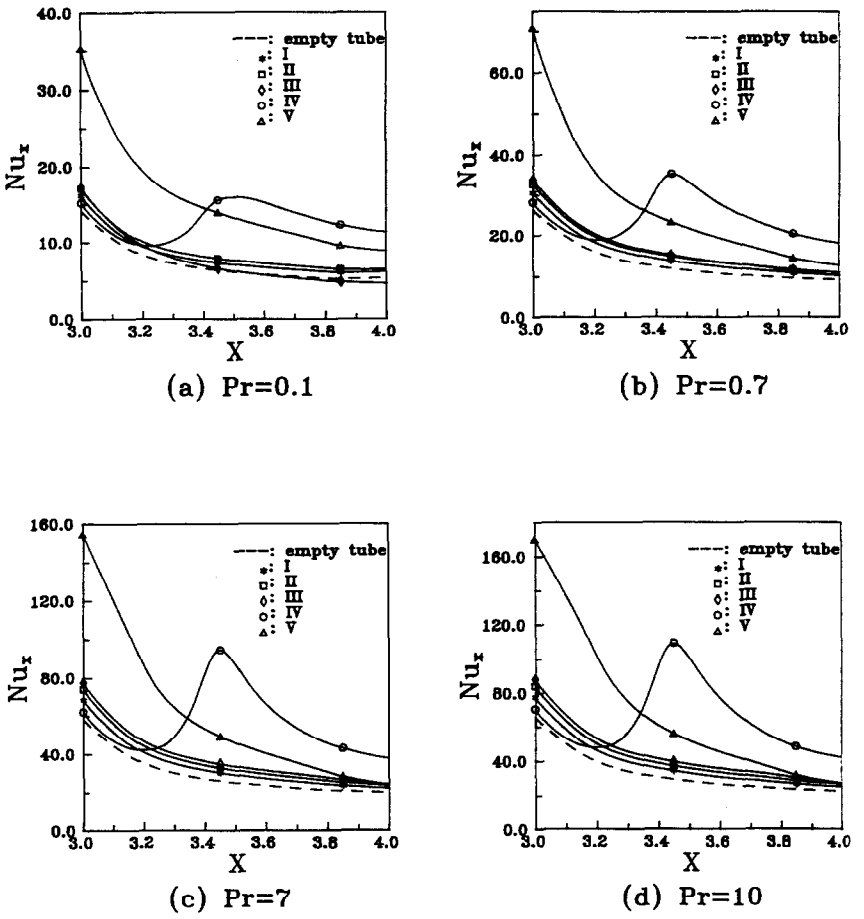

FIG. 9. Local Nusselt number distributions for $Re = 1000$ situation.

The constant pumping power method is used to compare the heat transfer rate between the tube with an inner tube insertion and the empty tube is under the condition of same input power and fixed heat-transfer surface area. The pumping power PP is defined as:

$$PP = \left(\frac{\dot{m}}{\rho}\right)\Delta p \tag{16}$$

which may be rearranged and written as:

$$PP = \left(\frac{\mu^3}{64\rho^2 d^2}\right)\left(\frac{\Delta p}{\rho u_m^2}\right) Re^3. \tag{17}$$

Since the first term on the RHS is a constant for the same fluid, the constant pumping power can be expressed as:

$$(f\,Re^3)_s = (f\,Re^3)_o \tag{18}$$

where the subscripts s and o denote the tube with an inner tube insertion and empty tube, respectively.

Since the pressure drop for empty tube can be represented in the form $f = 284.76/Re$, equation (18) becomes

$$(f\,Re^3)_s = (284.76\,Re^2)_o. \tag{19}$$

For a given Reynolds number Re_s of a case of the tube with an inner tube, the pressure drop f and temperature distribution can be obtained. Substituting Re_s and f into the LHS of equation (19), the Reynolds number of the empty tube on the RHS is determined. This Re of the empty tube is used to calculate the temperature distribution of the empty tube under the same conditions as the original case of Re_s. It should be noted that for the case of type V at $Re = 1000$, the calculated Re of the empty tube ($Re = 2426$) is higher than the critical Re of laminar flow ($Re_{cr} = 2300$). The assumption of laminar flow still holds at this Reynolds number for simplicity. Finally, the heat transfer rate ratios Q_s/Q_o can be computed by the following equations:

$$Q_s = [\dot{m}c(T_{bl} - T_c)]_s \tag{20}$$

$$Q_o = [\dot{m}c(T_{bl} - T_c)]_o \tag{21}$$

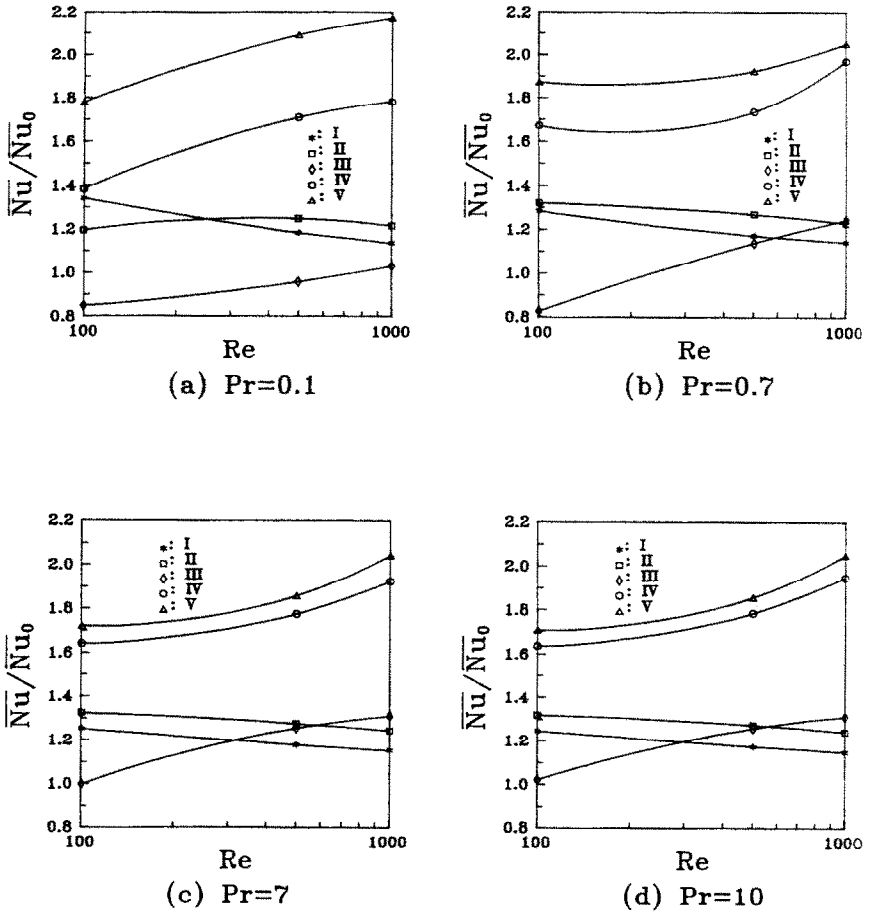

FIG. 10. Ratio of average Nusselt number with inner tube to that of empty tube.

$$T_{bl} = \frac{1}{\dot{m}_t}\int_0^{r_0} \rho u(r) Tr\, dr: \quad \text{bulk temperature at exit of outer tube.} \tag{22}$$

and

$$\frac{Q_s}{Q_o} = \frac{[(\theta_{bl}-\theta_c)]_s}{[(\theta_{bl}-\theta_c)]_o}. \tag{23}$$

The results of Q_s/Q_o are presented in Fig. 11. The values of Q_s/Q_o for types I, II, IV and V are greater than 1 except at low Prandtl number (= 0.1) and low Reynolds number (= 100). When Reynolds number increases, the values of Q_s/Q_o for types IV and V also increase no matter what the Prandtl number is. The maximum value of Q_s/Q_o of 1.491 can be attained for type V and 1.461 for type IV. The values of Q_s/Q_o for types I and II decrease, except for $Pr = 0.1$, with the increase of Re. For type III, the variations of the values of Q_s/Q_o with Reynolds number are opposite to those of the types I and II. In general, the trends of variation of Q_s/Q_o shown in Fig. 11 are similar to those of the constant flow rate evaluation shown in Fig. 10.

CONCLUSIONS

This study analyzes the effects on heat transfer enhancement when inserting an inner tube into a straight outer tube. The results can be summarized as follows:

(1) The Reynolds number influences the ratio of fluid deviation between inner and outer wall significantly.

(2) For a straight inner tube insertion, to obtain the higher heat transfer rate, the insertion position should depend on Peclet number. For low Peclet number, it should be placed near the center of the outer tube. As Peclet number increases, the position of the inner tube should be set closer to the outer wall to achieve a better heat-transfer performance.

(3) The insertion of an enlargement–contraction tube increases the ratio of fluid deviation greatly, so the heat transfer augmentation is the highest. The increase may reach 2.1 and 1.5 under the condition of constant flow rate and constant pumping power, respectively.

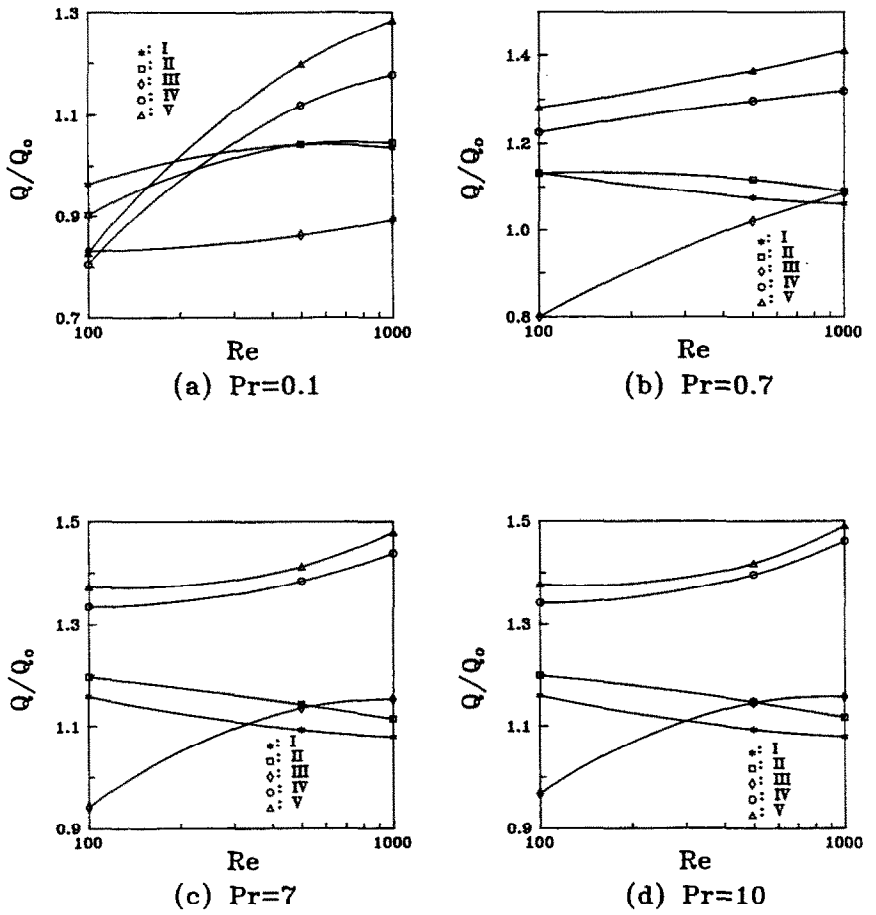

FIG. 11. Ratio of heat transfer with inner-tube insertion for constant pumping power.

Acknowledgement—The support of this work by National Science Council, Taiwan, R.O.C. under contract NSC82-0401-E-009-389 is gratefully acknowledged.

REFERENCES

1. A. E. Bergles, Recent developments in convective heat-transfer augmentation, *Appl. Mech. Rev.* **26**, 675–682 (1973).
2. A. E. Bergles, Survey and evaluation of techniques to augment convective heat and mass transfer. In *Progress in Heat and Mass Transfer*, Vol. 1, pp. 331–424. Pergamon Press, Oxford (1969).
3. T. M. Nguyen, J. M. Khodadadi and N. S. Vlachos, Laminar flow and conjugate heat transfer in rib roughened tubes, *Numer. Heat Transfer* **15**, 165–179 (1989).
4. D. L. Gee and R. L. Webb, Forced convection heat transfer in helically rib-roughened tubes, *Int. J. Heat Mass Transfer* **23**, 1127–1136 (1980).
5. S. V. Patankar, M. Ivanovic and E. M. Sparrow, Analysis of turbulent flow and heat transfer in internally finned tubes and annuli, *ASME J. Heat Transfer* **101**, 29–37 (1979).
6. G. J. Rowley and S. V. Patankar, Analysis of laminar flow and heat transfer in tubes with internal circumferential fins, *Int. J. Heat Mass Transfer* **27**, 553–560 (1984).
7. E. M. Sparrow and A. T. Prata, Numerical solutions for laminar flow and heat transfer in a periodically convergent–divergent tube with experimental confirmation, *Numer. Heat Transfer* **6**, 441–461 (1983).
8. A. T. Prata and E. M. Sparrow, Heat transfer and fluid flow characteristics for an annulus of periodically varying cross section, *Numer. Heat Transfer* **7**, 285–304 (1984).
9. A. K. Agrawal and S. Sengupta, Laminar flow and heat transfer in blocked annuli, *Numer. Heat Transfer* **15**, 489–508 (1989).
10. S. V. Patankar, *Numerical Heat Transfer and Fluid Flow*, p. 90. Hemisphere, New York (1980).
11. R. Peyret and R. D. Taylor, *Computational Methods for Fluid Flow*, p. 160. Springer, New York (1983).
12. E. M. Sparrow, B. R. Baliga and S. V. Patankar, Heat transfer and fluid flow analysis of interrupted-wall channels, with applications to heat exchangers, *J. Heat Transfer* **99**, 4–11 (1977).
13. E. M. Sparrow and C. H. Liu, Heat-transfer, pressure-drop and performance relationships for in-line, staggered, and continuous plate heat exchangers, *Int. J. Heat Mass Transfer* **22**, 1613–1625 (1979).